Nanoscale

COMMUNICATION

View Article Online
View Journal | View Issue

Cite this: *Nanoscale*, 2024, **16**, 12411

Received 3rd May 2024,
Accepted 24th May 2024

DOI: 10.1039/d4nr01911c

rsc.li/nanoscale

Cu–Pd bimetal-decorated siloxene nanosheets for semi-hydrogenation of acetylene†

Xinyi Pei,‡[a] Dake Zhang,‡[a] Rui Tang,[b] Shenghua Wang,[a] Chengcheng Zhang,[a] Wentao Yuan[b] and Wei Sun *[a]

Metallic Pd has been proved highly promising when paired with Cu for industrially important acetylene semi-hydrogenation. Herein, we demonstrate that high-surface-area siloxene can feasibly enable alloying between Pd and Cu *via* room-temperature reduction with Si–H bonds. Unprecedentedly small Cu nanoparticles with isolated Pd were *in situ* loaded on siloxene, addressing the core problem of low selectivity of Pd and low activity of Cu. This devised structure outclassed the traditional impregnated SiO_2 in every aspect of the catalytic performance for the semi-hydrogenation of acetylene under industry conditions, with a 91% acetylene conversion and an impressive 93% selectivity to ethylene at 200 °C, and showed long-term stability with negligible activity decay at this harsh temperature. This work provides new insights for the design of economic bimetallic loaded catalysts for balancing the activity–selectivity dilemma, demonstrating the viability of siloxene as both a synthetic reagent and a carrier material for efficient catalysis.

1. Introduction

Ethylene is an essential chemical raw material that indicates the level of industrial development of a country.[1,2] At present, the production of ethylene is mainly through the naphtha cracking method, which leads to a small amount of acetylene (0.5%–3.0%) in the ethylene stream, causing poisoning of the downstream polymerization reaction, so selective semi-hydrogenation of the trace amount of acetylene to ethylene while avoiding further ethylene hydrogenation to the undesired ethane has received widespread attention.[3–8]

Semi-hydrogenation of acetylene can be efficiently catalyzed by supported precious metal nanocatalysts, exemplified by Pd-based catalysts, owing to their strong ability to absorb and dissociate hydrogen.[9–14] However, while pure Pd-based catalysts enable high acetylene conversion, they often lead to undesired over-hydrogenation and polymerization byproducts, which would cause a decrease in the ethylene selectivity. Thus, a second metal is often added to Pd-based catalysts to form bimetallic alloy catalysts and improve the atom efficiency and the selectivity of ethylene.[15–17] This strategy is exemplified by replacing some or most of the precious Pd with the cheap and abundant copper (Cu, 3d-transition metal) to shift down the d-band of Pd and disperse its active sites, leading to weakened adsorption of ethylene to avoid over-hydrogenation.[18–22] Despite the efficacy of this strategy, previous efforts have predominantly been focused on only the metals, while there have been few explorations of functional support materials beyond the traditional ones like SiO_2 and Al_2O_3.

In recent decades, two-dimensional (2D) materials have shown significant promise for the conversion of small energy-related molecules, and have brought new opportunities to enhance charge transfer, provide abundant active surface sites, and confine metals between the layers for strong metal–support interactions.[23,24] As the second earth-abundant element, silicon in the 2D form deserves particular research interest in heterogeneous catalysis.[25,26] In recent studies, the synthesis strategies of 2D Si have advanced to the scalable production of structures with reductive Si–H bonds to deposit catalytic metals *in situ* on the surface, and a high surface area for the decoration of high amounts of highly dispersed nanoparticles to achieve better catalytic performances in heterogeneous reactions.[27–29] 2D silicon support can also improve the stability of the metal, which prevents the deactivation of catalysts. For instance, Cu nanoparticles embedded in 2D Si have been proved highly stable for the high-temperature reverse water–gas shift reaction,[26] and Ni nanoparticles sandwiched in siloxene nanosheets slowly released the active sites and exhibited an anti-coke pathway for CO_2 methanation.[29]

[a]*State Key Laboratory of Silicon Materials and Advanced Semiconductor Materials, and School of Materials Science and Engineering, Zhejiang University, Hangzhou, Zhejiang 310027, People's Republic of China. E-mail: sunnyway423@zju.edu.cn*
[b]*Center of Electron Microscopy and State Key Laboratory of Silicon Materials, School of Materials Science and Engineering, Zhejiang University, Hangzhou, 310027, China*

†Electronic supplementary information (ESI) available. See DOI: https://doi.org/10.1039/d4nr01911c

‡These authors contributed equally to this work.

Herein, we report siloxene—the partially oxidized form of 2D Si—with a devised synthesis and structure that can simultaneously reduce both Pd and Cu cations and form a novel supported PdCu bimetallic nanoalloy catalyst (PdCu/siloxene). Highly isolated Pd sites in ultrasmall Cu nanoparticles were well dispersed in the high-surface-area siloxene, exhibiting excellent catalytic performance for the semi-hydrogenation of acetylene, the archetype reaction that can be accelerated selectively with Pd–Cu alloy. At 200 °C, the PdCu/siloxene catalytic structure with a relatively low Pd ratio (0.1 wt% Pd, 3.2 wt% Cu) exhibited ~91% conversion of C_2H_2 and ~93% C_2H_4 selectivity at 50 mL min^{-1} of 1.0% C_2H_2, 10% H_2 with N_2 balance, which significantly outperformed the conventional Pd–Cu alloy supported with ordinary SiO_2 (PdCu/SiO_2). In addition, the siloxene support enabled excellent stability during the long-time hydrogenation test (over 30 hours).

2. Experimental section

2.1 Catalyst preparation

2.1.1 Preparation of siloxene support. The siloxene support was synthesized with an improved etching-exfoliation method. First, to remove the observable amount of bulk Si in the $CaSi_2$ precursor, which would be the major impurity and redundant content for further synthesis, $CaSi_2$ was etched using a 5 M NaOH solution. 2.0 g of $CaSi_2$ was stirred in 200 mL of NaOH solution at room temperature for 14 hours. Then, 1.0 g of the resulting solid recovered was mixed with 100 mL of pre-diluted hydrochloride acid (1 M) in a round bottom flask and stirred at 30 °C for 4.5 days in an N_2 atmosphere. After that, the remaining solid was separated from the solvent by centrifugation, washed with ethanol, and dried under vacuum.

2.1.2 Preparation of PdCu/siloxene catalysts. PdCu/siloxene catalyst was synthesized using the liquid-phase reduction method, which reduced the metal ions with Si–H on siloxene. Typically, 60 mg of siloxene was mixed with 1.46 mL of $NaPdCl_4$ (0.5 mg mL^{-1}) and 0.60 mL of $Cu(NO_3)_2{\cdot}2H_2O$ (20 mg mL^{-1}) aqueous solution at room temperature, and was sonicated for 3 min. The solid was collected by centrifuging and washed with ethanol. The Pd and Cu loadings determined by Inductively Coupled Plasma Optical Emission Spectroscopy (ICP-OES) were 0.1 and 3.2 weight % (wt%), respectively. Then, the sample was dried in the vacuum oven at 40 °C and then calcinated at 400 °C for 2 h in a muffle furnace before the catalytic evaluation process.

2.1.3 Preparation of PdCu/siloxene-300 and PdCu/SiO_2 catalysts. Two control samples, PdCu/siloxene-300 and PdCu/SiO_2, were synthesized with the conventional impregnation method. For PdCu/siloxene-300, 60 mg of siloxene was first calcinated at 300 °C for 2 h to remove the Si–H bonds, then mixed with $NaPdCl_4$ and $Cu(NO_3)_2{\cdot}2H_2O$ solution. The amounts of metals for impregnation were determined to be consistent with the actual loading amounts of metals in PdCu/siloxene. The resulting suspension was continuously stirred at 120 °C to remove the solvent and dry the sample. Then it was calcinated at 400 °C in the air for 2 h in a muffle furnace. The synthesis of PdCu/SiO_2 was similar to that of PdCu/siloxene-300, except that the siloxene pre-heated at 300 °C was replaced with a commercial SiO_2 support, which was purchased from Alfa Aesar (high surface area, 0.125 inch pellets, 250 m^2 g^{-1}).

2.2 Structural characterizations

Fourier-transform infrared (FTIR) spectroscopy was performed on a Bruker Alpha FTIR spectrometer fitted with a universal attenuated total reflectance sampling accessory. The actual metal loadings of the catalysts were analyzed by ICP-OES (i CAP Pro X, Thermo Fisher). X-ray diffraction (XRD) experiments were performed with an XRD-700 X-ray diffractometer from Shimadzu and the scanning angle (2θ) was 10–80°. X-ray photoelectron spectroscopy (XPS) was conducted using a Thermo Scientific K-Alpha. Al Kα radiation ($h\nu$ = 1486.6 eV) was used as the excitation source. The binding energy of the spectra was calibrated using the C 1s peak at 284.8 eV. The specific surface area was measured by the Brunauer–Emmett–Teller (BET) method. Scanning electron microscopy (SEM) images were recorded using a HITACHI S4800 scanning electron microscope. Transmission electron microscopy (TEM) images and energy dispersive X-ray spectroscopy (EDS) mappings were obtained on an FEI Tecnai G^2 F20 S-TWIN transmission electron microscope with an accelerating voltage of 200 kV. High-angle annular dark-field scanning transmission electron microscopy (HAADF-STEM) images were taken on Titan G^2 80–200 ChemiSTEM, FEI.

The hydrogen temperature-programmed reduction (H_2-TPR) tests were conducted on a Bel Cata II analyzer (MicrotracBEL) to study the interaction between active components and carriers. In the H_2-TPR experiments, 20 mg of catalyst was placed in a tubular reactor and pre-treated at 400 °C for 30 min under an Ar flow. After being cooled to room temperature, the reactor was switched to 10% H_2/Ar. After that, the reactor was heated to 800 °C at a heating rate of 10 °C min^{-1} and the signal of the gas product was recorded online with a TCD (Agilent). Raman spectroscopy measurements were carried out on a LabRam HR Evolution. Thermogravimetric mass spectrometry (TG-MS) was performed on a Netzsch TG-MS (LFA467) instrument in a N_2 atmosphere in the range of 50–600 °C with a ramp rate of 10 °C min^{-1} to determine the content of the organics in the catalysts.

2.3 Catalytic performance evaluation

The catalytic performance of the three sorts of catalysts was evaluated by the selective hydrogenation of acetylene experiments in a fixed-bed quartz reactor. For each test, 30 mg of catalyst was held in place by quartz wool and then loaded into a reactor tube. Before the catalytic test, the catalyst was pre-reduced by 10 mL min^{-1} H_2 at 300 °C for 1 h with a ramping rate of 10 °C min^{-1} and then cooled to room temperature in H_2 atmosphere. Then the inlet flow was switched to reaction gases (1.0% C_2H_2 and 10.0% H_2, with N_2 balance) with a total flow of 50 mL min^{-1}, and the reactor temperature was set from 80 °C to 200 °C, with a 100 min response time for each temp-

erature. The apparent activation energy (E_a) was determined with the same feed gas composition; to make sure the reaction rate was independent of the products and minimize the concentration gradients along the fixed-bed quartz reactor, the number of catalysts was reduced to 20 mg (mixed with 10 mg quartz sand) to keep the acetylene conversion below 20%.

For the stability tests, 30 mg of catalyst was mixed with 170 mg of quartz sand (40–60 mesh), which could buffer the flow and prevent clogging in the reactor tube. The reaction temperature of semi-hydrogenation of acetylene was set at 200 °C and the other reaction conditions remained the same. The stability test for PdCu/siloxene lasted over 20 hours.

The outlet products at the reactor were analyzed using an online gas chromatograph (GC-7980) equipped with a thermal conductivity detector (TCD) and a flame ionization detector (FID) to identify different gas products. The conversion of acetylene and selectivity toward ethylene were defined as follows:

$$C_2H_2\ \text{conversion} = \frac{F_{C_2H_2(\text{inlet})} - F_{C_2H_2(\text{outlet})}}{F_{C_2H_2(\text{inlet})}} \times 100\% = \frac{\frac{C_{C_2H_2(\text{inlet})}}{C_{N_2(\text{inlet})}} - \frac{C_{C_2H_2(\text{outlet})}}{C_{N_2(\text{outlet})}}}{\frac{C_{C_2H_2(\text{inlet})}}{C_{N_2(\text{inlet})}}} \times 100\%$$

$$C_2H_4\ \text{selectivity} = \frac{F_{C_2H_4(\text{outlet})}}{F_{C_2H_2(\text{inlet})} - F_{C_2H_2(\text{outlet})}} \times 100\% = \frac{\frac{C_{C_2H_4(\text{outlet})}}{C_{N_2(\text{outlet})}}}{\frac{C_{C_2H_2(\text{inlet})}}{C_{N_2(\text{inlet})}} - \frac{C_{C_2H_2(\text{outlet})}}{C_{N_2(\text{outlet})}}} \times 100\%$$

where F represents the mole flow rate of each substance in the inlet gas or outlet gas (mol min^{-1}) and C represents the concentration of reactants or products (%).

To verify the catalytic performance of PdCu/siloxene under industrial conditions, we also conducted tests with the gas composition 1.0% C_2H_2, 10.0% H_2, and 20% C_2H_4, with N_2 balance, and the total stream flow was 50 mL min^{-1}.

3. Results and discussion

3.1 Characterization of the catalyst support materials

As shown in the synthetic scheme in Fig. 1a, we successfully prepared the high-surface-area siloxene by an exfoliation method.[23] We started with the commercial $CaSi_2$ for the synthesis, and pretreated it with 5 M NaOH to remove the substantial amount of bulk Si and then exfoliated the dried products with 1 M HCl for 4.5 days, which separated the silicon layers as a low-cost method. As a result, the porous and stratified structure of siloxene can be observed in Fig. S1,† which was conducive to providing more active adsorption sites in the subsequent catalyst preparation process. As the exfoliation proceeded, Si–H bonds (640 cm^{-1} and 2110 cm^{-1}) were generated, confirmed by Fourier transform infrared (FTIR) spectroscopy (Fig. 1b), which could be leveraged for reductive deposition of Pd and Cu ions.[27,28,30] As expected, PdCu/siloxene exhibited significant reduced signals of Si–H bonds, indicative of their consumption for reducing Pd and Cu ions.

3.2 Structural characterizations of catalysts

The successful loading of both Pd and Cu in the PdCu/siloxene bimetallic metal catalyst was confirmed by ICP-OES. As shown in ESI Table S1,† the loadings of Pd and Cu were 0.1 wt% and 3.2 wt% in a typical sample, respectively. As shown in Fig. S1c and S1d,† the porous and stratified structure of siloxene remained the same after the Pd, Cu loading, but the metal nanoparticles may be ultrasmall and thus not discernible in these SEM images.

To reveal the metal sites, transmission electron microscopy (TEM) was employed. As shown in Fig. 1c, the nanoparticles are ultrasmall, uniform, and narrowly dispersed on the siloxene support and the average size of nanoparticles distinguished in the TEM images is about 2.2 ± 0.8 nm (Fig. 1d). Moreover, the EDS elements mapping images (Fig. 1e) collected to provide the composition and elemental distribution information for PdCu/siloxene also support the conclusion that Pd and Cu are both present and dispersed on the siloxene support. In addition, the HAADF-STEM image (Fig. 1f) shows that two kinds of atoms are present with different contrasts within a particle. Considering that the loading of Cu in the process of preparation is much higher than that of Pd, and the atomic number of Pd is also higher than Cu, the atoms with the higher brightness in the HAADF-STEM image are possibly Pd. Thus, it may be speculated that the seemingly isolated Pd atoms are surrounded by Cu atoms in the prepared bimetallic catalyst. The HRTEM image (Fig. 1g) also illustrates slightly different lattice parameters in the different areas of PdCu/siloxene, among which the lattice parameter of 0.314 nm corresponds to the (111) crystal face of Si and the lattice parameter of 0.209 nm corresponds to the (111) crystal face of Cu. Moreover, the lattice parameter of 0.216 nm is between those of Pd (0.225 nm) and Cu (0.209 nm), which may correspond to the formation of a PdCu alloy.

To further verify the formation of a PdCu alloy, the XRD patterns of siloxene and PdCu/siloxene were investigated (Fig. 2a). However, the XRD pattern of PdCu/siloxene reveals no evident plane diffraction peaks assigned to facets of Pd and Cu, which may be due to its low loading amount (below the detection limit), its small nanoparticle size or its highly dispersed state. Thus, XPS measurement was applied to study the surface chemical and electronic structures of Pd and Cu in PdCu/siloxene. The XPS survey spectrum displays the existence of Cu element (Fig. 2b); however, the Pd signal is too weak to be shown. The high-resolution Cu 2p and Pd 3d XPS spectra of PdCu/siloxene and two mono-metallic control samples Cu/siloxene and Pd/siloxene were thus collected, and are shown in Fig. 2c and d. Two main characteristic peaks at 933.2 and 953.1 eV were observed for Cu/siloxene in the Cu 2p region, corresponding to Cu $2p_{3/2}$ and Cu $2p_{1/2}$ respectively, but they shifted to a slightly lower energy for PdCu/siloxene.

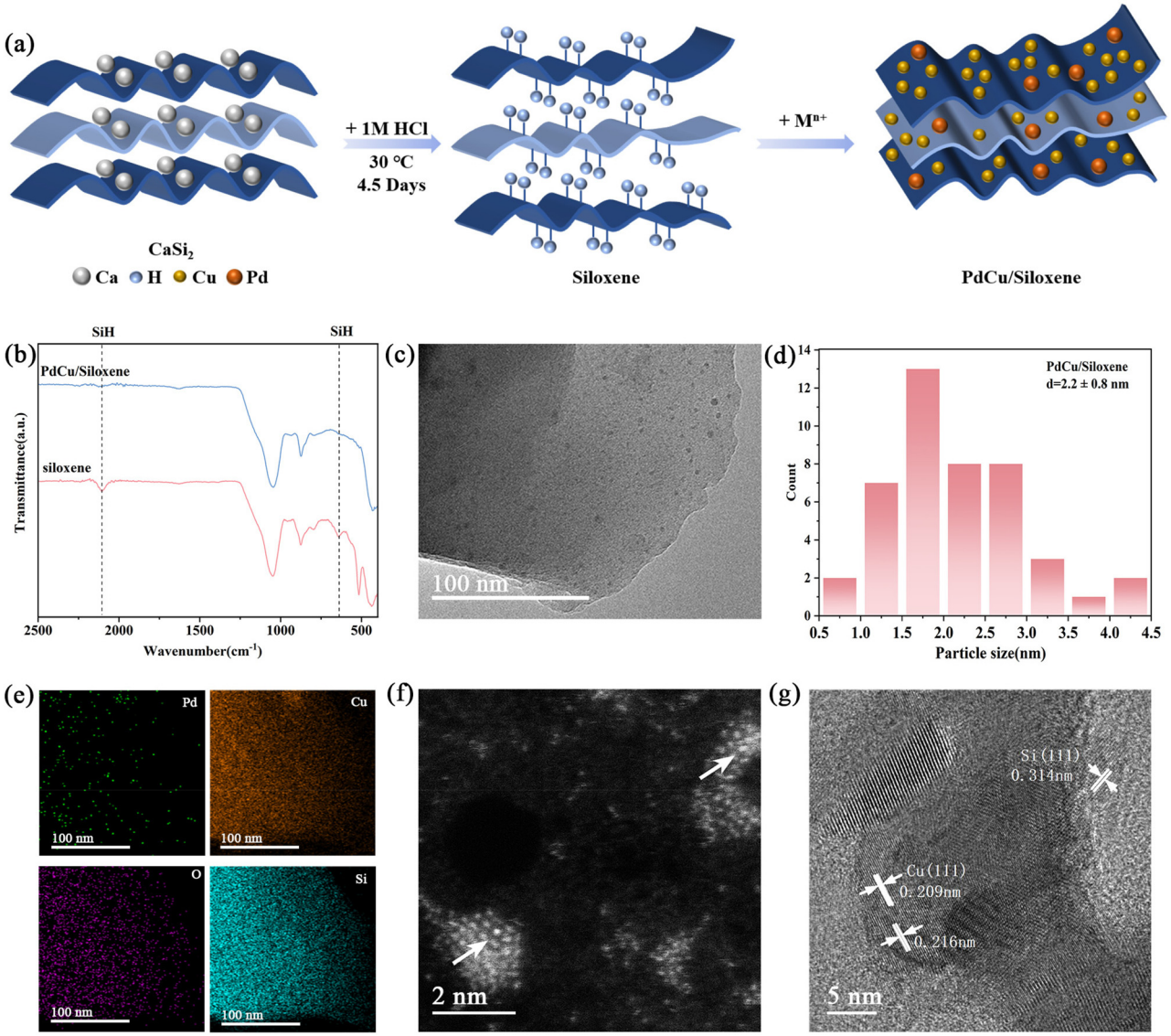

Fig. 1 (a) Schematic illustration of the synthesis of PdCu/siloxene. (b) FTIR spectrum of siloxene and PdCu/siloxene. (c) TEM image, (d) the diameter distributions, (e) EDS element mapping of Pd (green), Cu (orange), O (purple) and Si (cyan), (f) HAADF-STEM image and (g) HRTEM image of PdCu/siloxene.

Meanwhile, the Pd $3d_{5/2}$ and Pd $3d_{3/2}$ peaks in PdCu/siloxene at 335.7 and 341.1 eV exhibited a positive shift compared to Pd/siloxene. The opposite shift directions of Cu 2p and Pd 3d binding energies are mainly attributed to the electron interactions between Cu and Pd, which indicate the formation of PdCu alloy in PdCu/siloxene.[31,32]

3.3 Catalytic performance for acetylene semi-hydrogenation

In order to evaluate the catalytic performance of PdCu/siloxene for semi-hydrogenation of acetylene, the catalyst was tested in a lab-scale fixed-bed reactor with 1% acetylene, 10% hydrogen and nitrogen balance, and the total stream flow rate was 50 mL min^{-1}. Moreover, to demonstrate the superiority of our catalyst preparation method, we also prepared two control samples *via* the conventional impregnation method (PdCu/siloxene-300 and PdCu/SiO_2) and evaluated their catalytic performance under the same experimental conditions. In these two samples, as can be seen from the TEM and EDS mapping images in Fig. S2 and S3,† Pd and Cu nanoparticles were also successfully loaded. However, the average sizes of nanoparticles distinguished in the TEM images are about 7.7 ± 2.1 nm and 9.5 ± 3.3 nm for PdCu/siloxene-300 and PdCu/SiO_2 respectively, which are significantly larger than that of PdCu/siloxene (2.2 ± 0.8 nm). Moreover, on the SiO_2 support, the metal particles seem the biggest and with a wide distribution of size.

The BET results (Fig. S4†) showed that the surface area of PdCu/siloxene (106 m^2 g^{-1}) was slightly larger than that of PdCu/siloxene-300 (86 m^2 g^{-1}) but was smaller than that of PdCu/SiO_2 prepared with the commercial support (230 m^2 g^{-1}).

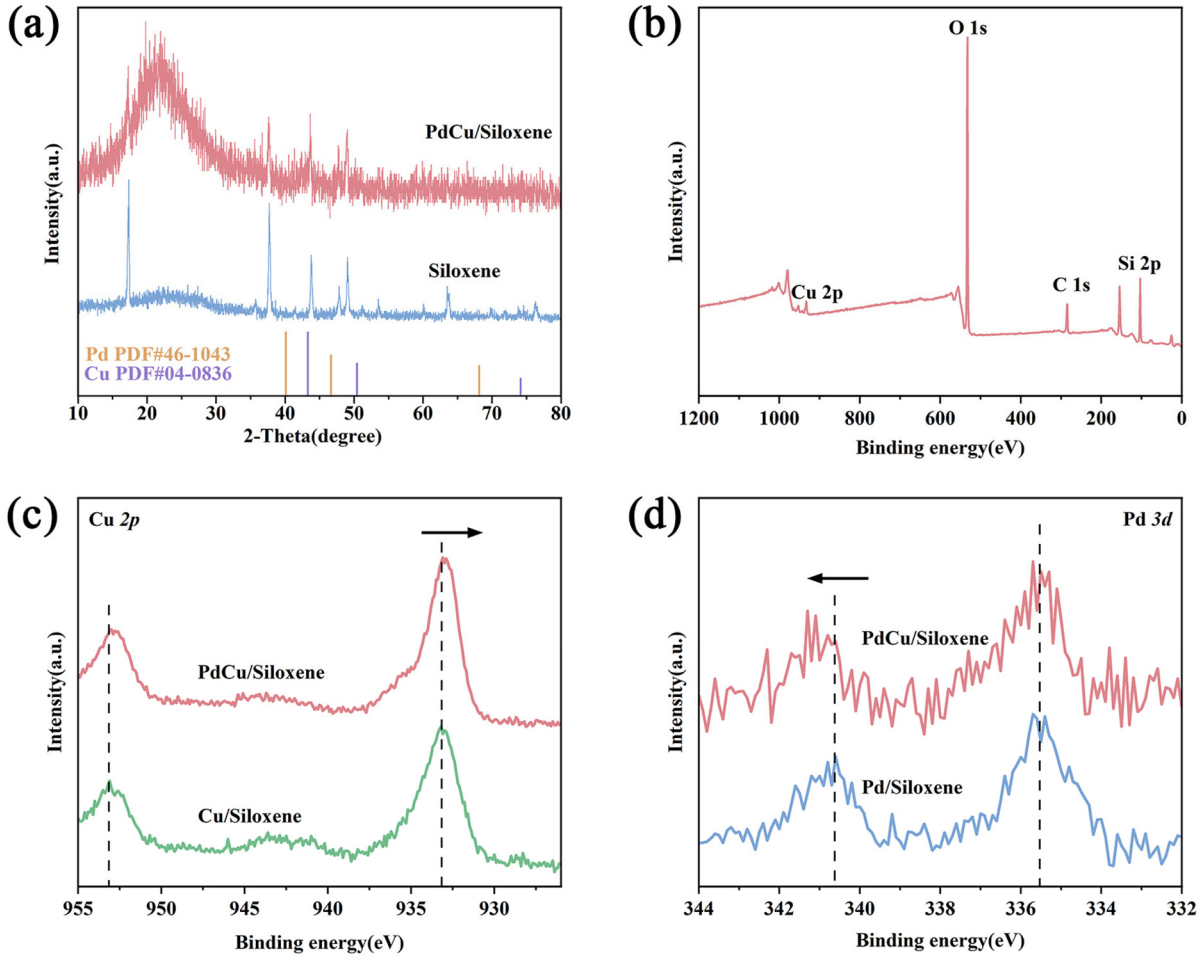

Fig. 2 (a) The XRD spectra of siloxene and PdCu/siloxene. (b) XPS survey spectra pf PdCu/siloxene. (c) Cu 2p XPS spectra of different catalysts, (d) Pd 3d XPS spectra of different catalysts.

In this regard, if the siloxene-supported catalyst can show better catalytic performance than the SiO_2-supported catalyst, it will further highlight the better loading ability of metal nanoparticles and the advantage of siloxene as an excellent support in the preparation of acetylene semi-hydrogenation catalysts.

Before the acetylene semi-hydrogenation evaluation, H_2-TPR experiments were conducted to investigate the capability of hydrogen reduction over the three catalysts, Fig. S5,† which showed the maximum losses at 228 °C, 219 °C, and 207 °C for PdCu/siloxene, PdCu/siloxene-300, and PdCu/SiO_2, respectively. Thus, a typical pre-reduction step at 300 °C in the reactor was performed to ensure the fresh metallic states of Pd and Cu. Besides that, the maximum loss temperature of PdCu/siloxene was the highest among three samples, which clarifies that the metals ought to form the strongest interaction with the siloxene support, which could be beneficial for the catalytic activity and stability.[33,34]

The activity of the pristine siloxene support was first excluded from 80 to 200 °C: the acetylene conversion of siloxene was always below 1%. The catalytic performance for semi-hydrogenation of acetylene over the three catalysts samples was further evaluated at different reaction temperatures, and the results are shown in Fig. 3a and b, showing that below 200 °C, with the increase in the test temperature, the acetylene conversion of PdCu/siloxene increased continuously and was the highest among the three samples, and at 200 °C the acetylene conversion and ethylene selectivity both exceeded 90%. The ethylene selectivity of PdCu/siloxene-300 is comparable with that of PdCu/siloxene. However, since the metals were loaded using the impregnation method rather than *in situ* reduction with Si–H bonds, the increased size of metal particles in PdCu/siloxene-300 led to inferior conversions at all temperatures compared with PdCu/siloxene. As for PdCu/SiO_2, its acetylene conversions were the lowest below 180 °C, which should be ascribed to the inhomogeneous and large size of the nanoparticles. Only when the reaction temperature reached as high as 200 °C was its conversion comparable with that of PdCu/siloxene. However, the ethylene selectivity decreased dramatically to ~53% at 200 °C due to the over-hydrogenation of ethylene. Besides that, as shown in Fig. 3c, PdCu/siloxene delivered the greatest yield of ethylene among

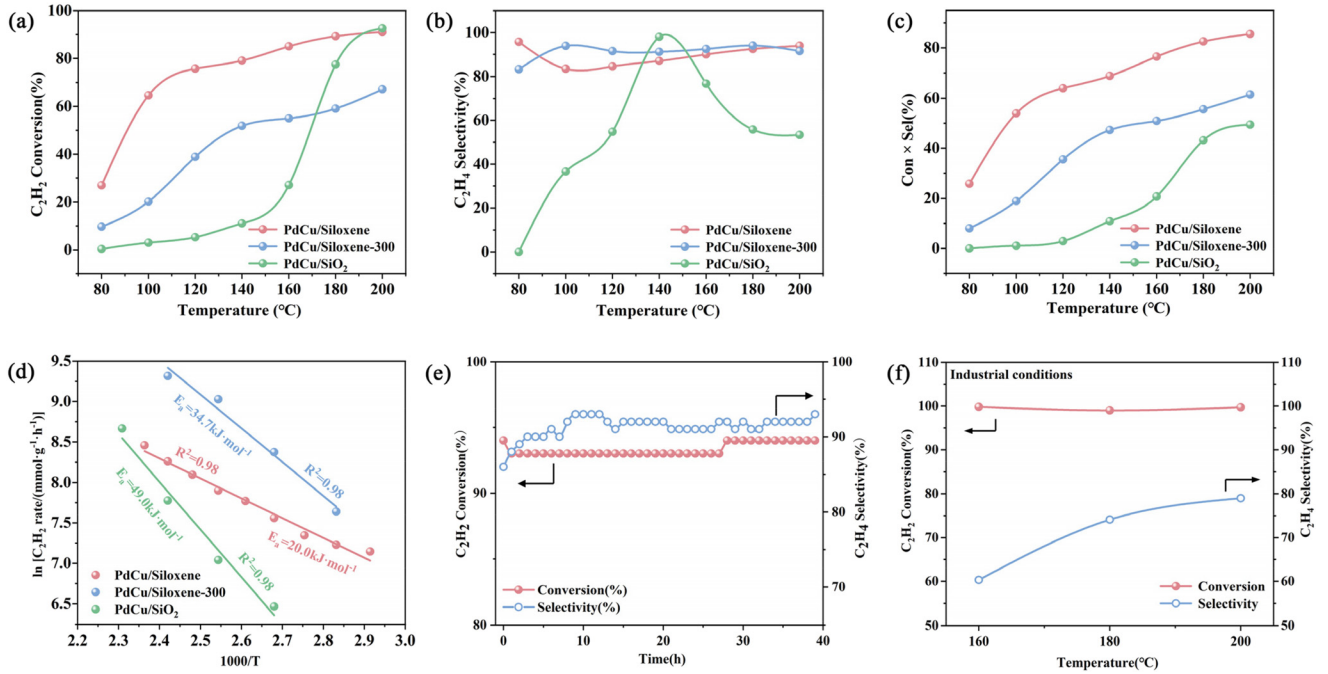

Fig. 3 (a) Acetylene conversion, (b) ethylene selectivity, (c) yield of ethylene and (d) Arrhenius plot fitting from the acetylene conversion rates over PdCu/siloxene, PdCu/siloxene-300 and PdCu/SiO_2. (e) Stability evaluation during a 39 hour test over PdCu/siloxene at 200 °C. (Reaction conditions: 1.0% C_2H_2 and 10.0% H_2 with N_2 balance, total flow of 50 mL min^{-1}.) (f) Acetylene conversion and ethylene selectivity over PdCu/siloxene under industrial conditions. (Reaction conditions: 1.0% C_2H_2, 10.0% H_2 and 20% C_2H_4 with N_2 balance, total flow of 50 mL min^{-1}.)

the three samples at all temperatures. At 200 °C, PdCu/siloxene shows a 91% acetylene conversion and an impressive 93% selectivity for ethylene, reaching an 86% yield of ethylene, which is significant for acetylene semi-hydrogenation. Furthermore, the mono-metallic catalysts Pd/siloxene and Cu/siloxene under the same testing conditions are far less effective, as shown in Fig. S6,† which demonstrates the necessity and advantages of both of the two metals. Moreover, the values of apparent activation energy (E_a) for the catalysts were derived by graphing ln [C_2H_2 conversion rate] *versus* 1000/*T*, according to Arrhenius plots. As shown in Fig. 3d, the apparent E_a for acetylene hydrogenation over PdCu/siloxene (20.0 kJ mol^{-1}) is much smaller than those over PdCu/siloxene-300 (34.7 kJ mol^{-1}) and PdCu/SiO_2 (49.0 kJ mol^{-1}), supporting the highly dispersed and ultrasmall particles of PdCu/siloxene having a significantly larger surface-to-volume ratio and being able to expose more Pd–Cu bimetallic sites which are particularly efficient for the effective semi-hydrogenation of acetylene.

The advantage of siloxene as the support material was also demonstrated by its excellent stability. As shown in Fig. 3e, during a long-time test (39 hours) at 200 °C, the catalytic activity of PdCu/siloxene could still maintain a relatively stable level: the acetylene conversion was always above 93%, and the selectivity of ethylene rose slightly at the beginning of the stability test and then fluctuated around ~91%. In comparison, the stabilities of PdCu/siloxene-300 and PdCu/SiO_2 are shown in Fig. S7;† PdCu/siloxene-300 exhibited an overall decent selectivity maintained below 90%, owing to the similar stabilizing effect of the support structure, but the acetylene conversion was far from excellent at 200 °C in the long-time test (20 hours). As for PdCu/SiO_2, although the initial acetylene conversion was higher than 88%, it showed an ever-decreasing trend with the reaction time, and its ethylene selectivity was always lower than 70%. To sum up, PdCu/siloxene not only has the overall best catalytic activity, ethylene selectivity, and yield over a wide temperature range, but also shows the best stability and performance among the three samples during the long-time test at a high operating temperature. It is also noteworthy that the existing literature has not reported such stable yet high performance at this harsh temperature (Table S2 in the ESI† [35–37]).

In order to further verify the catalytic performance of PdCu/siloxene under industrial conditions, we changed the reaction gas conditions to 1.0% C_2H_2, 10.0% H_2 and 20% C_2H_4, with N_2 balance and a total stream flow of 50 mL min^{-1}. As shown in Fig. 3f, when there was a significant amount of ethylene premixed in the reaction gas, although the ethylene selectivity of the prepared PdCu/siloxene catalyst was slightly sacrificed, the acetylene conversion remained at a high level. Additionally, the long-term test at 120 °C in such a gas environment for 20 hours of PdCu/siloxene also shows excellent stability with ~67% acetylene conversion and ~80% ethylene selectivity (Fig. S8†).

To further reveal the significant stability advantage of siloxene, we also characterized the catalysts collected after the acetylene semi-hydrogenation reaction. As shown in Fig. 4a, b and Fig S9,† the TEM images of PdCu/siloxene-tested and PdCu/SiO_2-tested were collected, and the particle size of PdCu/siloxene-tested remained the same as before, while the particle size of PdCu/SiO_2-tested increased from 9.5 ± 3.3 to 13.8 ±

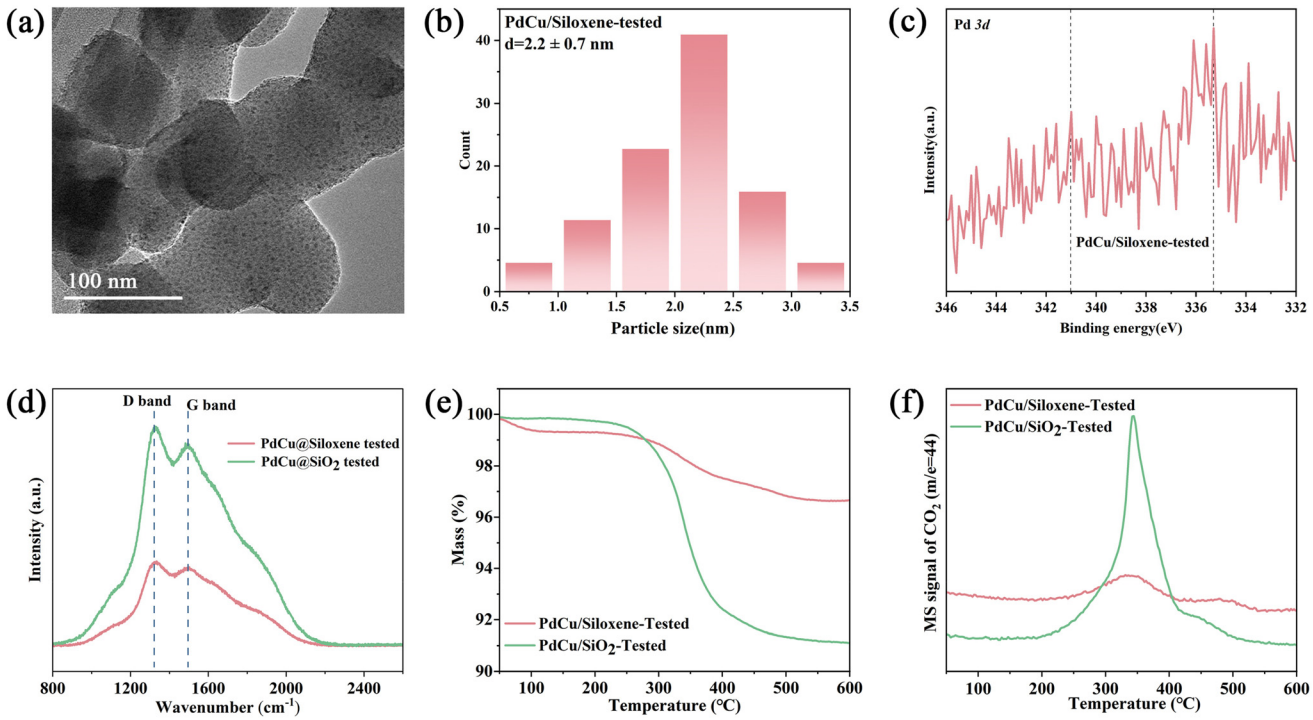

Fig. 4 (a) TEM image, (b) the diameter distributions, (c) Pd 3d XPS spectra of PdCu/siloxene-tested. (d) Raman spectra, (e) and (f) TG-MS curves of PdCu/siloxene-tested and PdCu/SiO_2-tested.

1.7 nm. Furthermore, the Pd 3d XPS scan spectra of PdCu/siloxene-tested (Fig. 4c) also showed that the binding energy of Pd $3d_{5/2}$ and Pd $3d_{3/2}$ remain unchanged, confirming the stability of the alloy.

To investigate the evolution of coke species over different catalysts, Raman spectra were collected after the semi-hydrogenation reaction. As shown in Fig. 4d, there was pronouncedly more carbon deposition generated on PdCu/SiO_2 during the acetylene semi-hydrogenation process. TG-MS experiments were further performed to determine the amount of deposited coke on the surface of catalysts (Fig. 4e and f), and the weight loss at ~350 °C is generally attributed to the combustion of carbonaceous species. The weight loss of PdCu/SiO_2-tested (8.71%) was much higher than that of PdCu/siloxene-tested (3.15%), which confirms that more carbon deposition was generated on PdCu/SiO_2 during the catalytic reaction. The deposited coke on the surface of PdCu/SiO_2 will hinder the semi-hydrogenation of acetylene and reduce the catalytic activity of the catalyst, which is consistent with the conclusion obtained by Raman spectra. The much less coking on PdCu/siloxene is in line with the literature reports that metals that are highly isolated and strongly interacted with or spatially restrained by the support have excellent anti-coking ability.[38,39]

4. Conclusions

In summary, we successfully synthesized a novel supported bimetallic PdCu/siloxene catalyst by direct liquid-phase reduction and *in situ* loading with siloxene. The small dosage of Pd was isolated within the ultrasmall Cu particles, which are well dispersed on siloxene. This size advantage is conferred by the strong reducing ability of Si–H bonds and the high-surface-area and porous structure of siloxene, merits that are not possessed by the traditional SiO_2 for impregnation. Leveraging such advantages, we have demonstrated that the bimetallic PdCu/siloxene catalyst performed superiorly in the acetylene semi-hydrogenation reaction, achieving 91% acetylene conversion and 93% ethylene selectivity at the same time at 200 °C. Moreover, PdCu/siloxene also performed with high activity and stability under the ethylene-rich industrial gas conditions. Besides that, challenging the coking problem at high operating temperatures, PdCu/siloxene also exhibited substantially high stability and anti-coking ability over a 39-hour test.

This work serves as a timely report that proves that the reducing siloxene epitomizing 2D functional structures could be an illustrious support material for loading bimetallic active sites, forming optimum catalysts for particular reactions that are efficiently driven with the concerted effects of two or even more metals. Additionally, since this work only focuses on the material synthetic advantage for catalytic performance, future work of interest could target the specific effect of the metal–siloxene interface on the catalytic mechanism. The purport lies in the exceptionally low apparent activation energy observed in the current test, and the recent works which discovered that the Si–O–metal interface could cause the favorable hetero-splitting of hydrogen for hydrogenation[40] and that

spatial confinement with siloxene can alter the reaction pathway. However, these could not be simply corroborated without sophisticated experimental design and apparatus, and thus deserve detailed and separate studies.

Author contributions

X. P. and D. Z. contributed to this work equally as co-first authors. W. S., X. P., and D. Z. carried out the synthesis and catalysis experiments, analyzed the data, and prepared the manuscript. R. T. and W. Y. carried out the TEM characterization and analysis. S. W. and C. Z. analyzed the catalytic data. All authors commented on the final manuscript.

Conflicts of interest

There are no conflicts to declare.

Acknowledgements

The authors acknowledge the support from the National Natural Science Foundation of China (52372233, 51902287, 52171019) and the Fundamental Research Funds for the Central Universities (226-2022-00200).

References

1 F. Studt, F. Abild-Pedersen, T. Bligaard, R. Z. Sørensen, C. H. Christensen and J. K. Nørskov, *Science*, 2008, **320**, 1320–1322.
2 K. Xie, K. Xu, M. Liu, X. Song, S. Xu and H. Si, *Mater. Today Catal.*, 2023, **3**, 100029.
3 J. H. Kang, E. W. Shin, W. J. Kim, J. D. Park and S. H. Moon, *J. Catal.*, 2002, **208**, 310–320.
4 W. Huang, J. R. McCormick, R. F. Lobo and J. G. Chen, *J. Catal.*, 2007, **246**, 40–51.
5 R. Shi, Z. Wang, Y. Zhao, G. I. N. Waterhouse, Z. Li, B. Zhang, Z. Sun, C. Xia, H. Wang and T. Zhang, *Nat. Catal.*, 2021, **4**, 565–574.
6 A. J. McCue and J. A. Anderson, *Front. Chem. Sci. Eng.*, 2015, **9**, 142–153.
7 Y. Wang, B. Liu, X. Lan and T. Wang, *ACS Catal.*, 2021, **11**, 10257–10266.
8 S. Zhou, L. Shang, Y. Zhao, R. Shi, G. I. N. Waterhouse, Y.-C. Huang, L. Zheng and T. Zhang, *Adv. Mater.*, 2019, **31**, 1900509.
9 Z. Yuan, A. Kumar, D. Zhou, J. Feng, B. Liu and X. Sun, *J. Catal.*, 2022, **414**, 374–384.
10 G. X. Pei, X. Y. Liu, X. Yang, L. Zhang, A. Wang, L. Li, H. Wang, X. Wang and T. Zhang, *ACS Catal.*, 2017, **7**, 1491–1500.
11 K. Liu, L. Jiang, W. Huang, G. Zhu, Y.-J. Zhang, C. Xu, R. Qin, P. Liu, C. Hu, J. Wang, J.-F. Li, F. Yang, G. Fu and N. Zheng, *Nat. Commun.*, 2022, **13**, 2597.
12 Z. Li, G. Lin, Y. Chen, Q. Xue, K. Feng and B. Yan, *Catal. Today*, 2023, **423**, 114253.
13 F. Huang, M. Peng, Y. Chen, X. Cai, X. Qin, N. Wang, D. Xiao, L. Jin, G. Wang, X.-D. Wen, H. Liu and D. Ma, *J. Am. Chem. Soc.*, 2022, **144**, 18485–18493.
14 K. Xie, K. Xu, M. Liu, X. Song, S. Xu and H. Si, *Mater. Today Catal.*, 2023, **3**, 100029.
15 F. Huang, Y. Deng, Y. Chen, X. Cai, M. Peng, Z. Jia, J. Xie, D. Xiao, X. Wen, N. Wang, Z. Jiang, H. Liu and D. Ma, *Nat. Commun.*, 2019, **10**, 4431.
16 F. Liu, Y. Xia, W. Xu, L. Cao, Q. Guan, Q. Gu, B. Yang and J. Lu, *Angew. Chem., Int. Ed.*, 2021, **60**, 19324–19330.
17 Q. Gao, Z. Yan, W. Zhang, H. S. Pillai, B. Yao, W. Zang, Y. Liu, X. Han, B. Min, H. Zhou, L. Ma, B. Anaclet, S. Zhang, H. Xin, Q. He and H. Zhu, *J. Am. Chem. Soc.*, 2023, **145**, 19961–19968.
18 G. Kyriakou, M. B. Boucher, A. D. Jewell, E. A. Lewis, T. J. Lawton, A. E. Baber, H. L. Tierney, M. Flytzani-Stephanopoulos and E. C. H. Sykes, *Science*, 2012, **335**, 1209–1212.
19 Q.-W. Ding, Q. Luo, L. Lin, X.-P. Fu, L.-S. Wang, G.-H. Yue, J. Lin, Q.-S. Xie and D.-L. Peng, *Rare Met.*, 2022, **41**, 2595–2605.
20 R.-Y. Miao, X.-X. Li, Q. Lei, H. Liu, Z.-H. Ma, X.-D. Liu, Z.-Y. Yin, Z.-B. Tang, L. Zhang and Y.-H. Tian, *Rare Met.*, 2022, **41**, 851–858.
21 Z. Wang, C. Li, G. Peng, R. Shi, L. Shang and T. Zhang, *Angew. Chem., Int. Ed.*, 2024, **63**, e202400122.
22 Z. Wang, L. Shang, H. Yang, Y. Zhao, G. I. N. Waterhouse, D. Li, R. Shi and T. Zhang, *Adv. Mater.*, 2023, **35**, 2303818.
23 Y. Su, S. Wang, L. Ji, C. Zhang, H. Cai, H. Zhang and W. Sun, *Nanoscale*, 2023, **15**, 154–161.
24 D. Deng, K. S. Novoselov, Q. Fu, N. Zheng, Z. Tian and X. Bao, *Nat. Nanotechnol.*, 2016, **11**, 218–230.
25 S. Wang, C. Wang, W. Pan, W. Sun and D. Yang, *Sol. RRL*, 2021, **5**, 2000392.
26 S. Wang, K. Feng, D. Zhang, D. Yang, M. Xiao, C. Zhang, L. He, B. Yan, G. A. Ozin and W. Sun, *Adv. Sci.*, 2022, **9**, 2104972.
27 C. Qian, W. Sun, D. L. H. Hung, C. Qiu, M. Makaremi, S. G. Hari Kumar, L. Wan, M. Ghoussoub, T. E. Wood, M. Xia, A. A. Tountas, Y. F. Li, L. Wang, Y. Dong, I. Gourevich, C. V. Singh and G. A. Ozin, *Nat. Catal.*, 2019, **2**, 46–54.
28 Q. Dai, Q. Meng, C. Du, F. Ding, J. Huang, J. Nie, X. Zhang and J. Chen, *Chem. Commun.*, 2020, **56**, 4824–4827.
29 X. Yan, W. Sun, L. Fan, P. N. Duchesne, W. Wang, C. Kübel, D. Wang, S. G. H. Kumar, Y. F. Li, A. Tavasoli, T. E. Wood, D. L. H. Hung, L. Wan, L. Wang, R. Song, J. Guo, I. Gourevich, F. M. Ali, J. Lu, R. Li, B. D. Hatton and G. A. Ozin, *Nat. Commun.*, 2019, **10**, 2608.
30 M. Ohashi, R. Yaokawa, Y. Takatani and H. Nakano, *ChemNanoMat*, 2017, **3**, 534–537.

31 Z. Wang, P. Tian, H. Zhang, K. Deng, H. Yu, Y. Xu, X. Li, H. Wang and L. Wang, *Inorg. Chem.*, 2023, **62**, 5622–5629.
32 Y. Ge, X. Wang, B. Huang, Z. Huang, B. Chen, C. Ling, J. Liu, G. Liu, J. Zhang, G. Wang, Y. Chen, L. Li, L. Liao, L. Wang, Q. Yun, Z. Lai, S. Lu, Q. Luo, J. Wang, Z. Zheng and H. Zhang, *J. Am. Chem. Soc.*, 2021, **143**, 17292–17299.
33 C. Xu, G. Chen, Y. Zhao, P. Liu, X. Duan, L. Gu, G. Fu, Y. Yuan and N. Zheng, *Nat. Commun.*, 2018, **9**, 3367.
34 S. Wang, K. Feng, D. Zhang, D. Yang, M. Xiao, C. Zhang, L. He, B. Yan, G. A. Ozin and W. Sun, *Adv. Sci.*, 2022, **9**, 2104972.
35 Q. Wu, C. Shen and C.-J. Liu, *Appl. Surf. Sci.*, 2023, **607**, 154976.
36 D. Zhou, G. Zhang, Y. Li, S. Liu, S. Han, Y. Zhou and W. Shen, *Chem. Eng. J.*, 2023, **472**, 144875.
37 S. Zou, B. Lou, K. Yang, W. Yuan, C. Zhu, Y. Zhu, Y. Du, L. Lu, J. Liu, W. Huang, B. Yang, Z. Gong, Y. Cui, Y. Wang, L. Ma, J. Ma, Z. Jiang, L. Xiao and J. Fan, *Nat. Commun.*, 2021, **12**, 5770.
38 J. Gu, M. Jian, L. Huang, Z. Sun, A. Li, Y. Pan, J. Yang, W. Wen, W. Zhou, Y. Lin, H.-J. Wang, X. Liu, L. Wang, X. Shi, X. Huang, L. Cao, S. Chen, X. Zheng, H. Pan, J. Zhu, S. Wei, W.-X. Li and J. Lu, *Nat. Nanotechnol.*, 2021, **16**, 1141–1149.
39 J. Zhang and F. Li, *Appl. Catal., B*, 2015, **176–177**, 513–521.
40 Y. Chai, G. Wu, X. Liu, Y. Ren, W. Dai, C. Wang, Z. Xie, N. Guan and L. Li, *J. Am. Chem. Soc.*, 2019, **141**, 9920–9927.